Turkish Journal of Electrical Engineering & Computer Sciences

http://journals.tubitak.gov.tr/elektrik/

Research Article

Turk J Elec Eng & Comp Sci
(2020) 28: 2895 – 2909

doi:10.3906/elk-1907-139

Optimized idling grid-connection strategy for synchronous condenser

Xiangjian SHI[1,2], **Heqing HUANG**[2], **Teng LIU**[2], **Wei MU**[2], **Jianfeng ZHAO**[1,*]
[1]Department of Electrical Engineering, School of Electrical Engineering, Southeast University, Nanjing, China
[2]NR Electric Co., Ltd, Nanjing, China

Received: 19.07.2019 • **Accepted/Published Online:** 29.05.2020 • **Final Version:** 25.09.2020

Abstract: The rise of large-scale HVDC transmission technology has introduced new requirements for dynamic reactive power compensation in power systems. The new generation of synchronous condensers is independent of grid voltage and does not need to be dragged by a coaxial prime mover, which can improve the dynamic reactive power compensation of the power grid. This new generation of synchronous condensers is dragged by the static frequency converter to a 105% rated speed, after which the static frequency converter logs out. In the process of idling, the excitation mode switching is completed and the unit is connected to the grid simultaneously. The synchronous device passively captures the connection-dot in the process of idling; as a result, increasing the grid-connection success rate and reducing the impact of grid connection become a pair of contradictions. In this paper, the boundary conditions of the new generation of synchronous condenser grid-connection systems are analyzed. These provide the basis for setting the synchronous device parameters. Furthermore, this paper proposes an optimized grid-connection strategy to ensure the new generation of synchronous condensers possesses good grid-connection characteristics.

Key words: Direct current transmission, synchronous condenser, static frequency converter, synchronous device, idling grid-connection

1. Introduction

With the rise of large-scale DC transmission technology, the problem of strong HVDC and weak AC systems is becoming increasingly serious [1]. At the same time, there is a large proportion of local grids receiving power, which is conducive to causing dynamic reactive power compensation shortages and voltage instability [2]. Ensuring safe and stable system operation requires a sufficient dynamic reactive power reserve capacity [3]. Especially, the problems of insufficient reactive power support at the receiving end, insufficient short-circuit capacity at the sending end [4], and insufficient reactive power facilities at the heavy load center [5] are becoming increasingly apparent.

In recent years, with the use of a large number of static VAR compensators, static synchronous compensators, and other static reactive power compensation devices, the application of domestic condensers has gradually decreased [6]. However, when a large system voltage amplitude sag occurs, a static reactive power compensation device will reduce the reactive power output capacity [7]. In contrast, the reactive power output of the new generation of synchronous condensers (SC) does not depend on the system voltage. [8] By optimizing the parameters of the unit body and control strategy of the excitation system, the dynamic reactive power response performance of the unit can be greatly improved; this is advantageous for the voltage stability of a power

*Correspondence: jianfeng_zhao@seu.edu.cn

grid, especially for the safe operation of DC converter stations [9]. This approach has more advantages than traditional static reactive power compensation devices [10]. The effective placement of a synchronous condenser can reduce the probability of commutation failure in a DC converter station [11], improve the stability margin of a converter station, and increase the transmitted power of DC engineering [12]. As a result, the installation of synchronous condensers in centralized areas of wind power and other new energies can effectively meet the reactive power compensation requirements of the power grid [13].

At present, the new generation 300 MVAR condenser adopts a static frequency converter (SFC) as the soft start system, which can preserve the coaxial prime mover and increase the stability of the system [14]. At the same time, in order to reduce costs, the SFC output transformer is omitted; however, this causes some difficulties with the unit grid connection [15]. The whole operation process of SC includes three stages: start-up stage with SFC, idling grid-connection stage and reactive power regulation stage. The SFC accelerates the SC to 105% rated speed in the start-up stage with SFC. Dynamic behaviors and control methods of the start-up stage with SFC are compared and analyzed in [16, 17]. The SFC logs out and the SC is connected to the power grid in the idling grid-connection stage. The constraint condition and success rate of grid-connection are studied in [18]. In the reactive power regulation stage, the SC ensures the safe and stable operation of the power grid [19].

This paper focuses on the research of the idling grid-connection stage, and analyzes the generation mechanism of the grid-connection problem of the new generation synchronous condenser. Through simulation experiments, it was found that the idling rate can be controlled by changing the excitation current. Consequently, according to the requirements of frequency difference and angle difference, an optimized grid-connection strategy is proposed. Further, the effectiveness and feasibility of the proposed strategy are verified using the RTDS platform.

2. Idling grid-connection problem

Figure 1 shows a wiring diagram of the primary circuit adopted by the 300 MVAR condenser project in China. There is no booster transformer on the output side of the SFC. When the SFC logs out (the IPB switch is off in the figure), the terminal voltage amplitude of the unit will not exceed the voltage-limiting value of the SFC output side (less than 3 kV). Therefore, before the unit is connected to the grid (RCB in Figure 1 is a grid-connection switch), the SFC must not be in operation, so that the excitation system can establish a rated terminal voltage of 20 kV to meet the voltage condition for grid connection. However, the SFC limit will cause the condenser to lose the primary power and idle. As a result, the system speed will decrease, and the frequency difference and angle difference will increase.

In order to solve the above contradiction, the following grid-connection strategy can be adopted: the SFC accelerates the unit to 105% rated speed (approximately 3150 rpm) and then logs out, and the ICB and IPB are disconnected. In the process of idling, the excitation system changes from the start-up excitation to the main excitation and establishes the rated terminal voltage. At the same time, the quasi-synchronous device captures the synchronization point and connects the unit to the grid. Because there is no prime mover in the idling grid-connection process, the synchronous device can only passively capture grid-connection points. Therefore, the conditions of synchronous grid connection must be studied to provide a basis for determining the parameters.

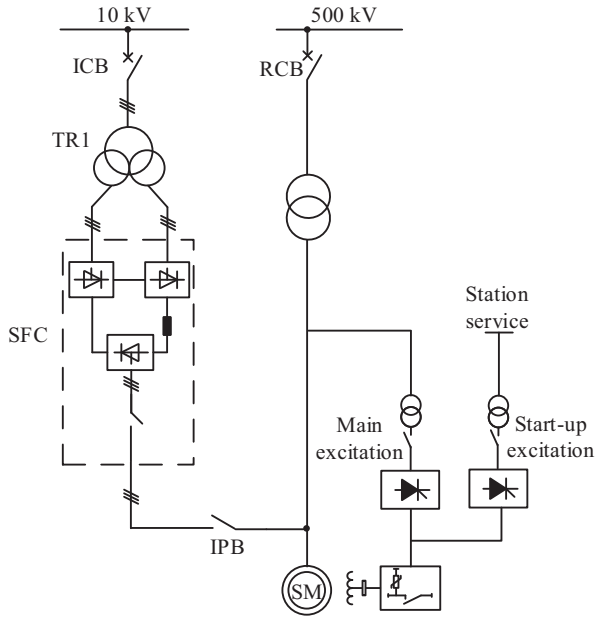

Figure 1. The illustrative start-up, excitation control and grid-connection system of the 300 MVAR synchronous condenser.

3. Analysis of grid connection conditions

3.1. Analysis of idle speed process

The idle process can be simulated by software according to the actual electrical, mechanical, and loss parameters of the condenser, as shown in Figure 2.

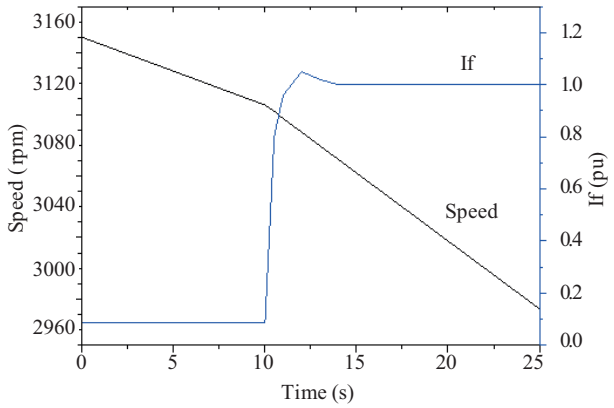

Figure 2. Relationship between the excitation current and the condenser speed during the idling process.

When the excitation system does not output a no-load rated excitation current, the unit speed decreases by approximately 4.4 rpm/s. When the main excitation does output a no-load rated excitation current, the losses of the main transformer and excitation transformer increase accordingly. The idling rate of the unit also clearly increases, and the unit speed decreases by approximately 8.82 rpm/s.

Based on the simulation results, the system idling speed is accelerated by the increase in total loss, and the transition in idling speed from 3150 rpm to 3000 rpm requires only approximately 20 s. Therefore, along with the main excitation output no-load rated excitation current, the idling speed process will be accelerated. If the system is not connected to the grid before 3000 rpm, the relationship between rotation speed and time can be approximately described as shown in Figure 3. From t_0 to t_1, the system completes the SFC exit, switch operation, and other processes. At time t_1, the main excitation begins to function, and at time t_2, the excitation current approaches the no-load rated excitation current, and the transition process is completed. The increase in excitation current accelerates the idling speed of the unit, and at time t_2, the unit enters the idling speed stage after excitation is established. At time t_3, the speed changes to a rated speed of 3000 rpm.

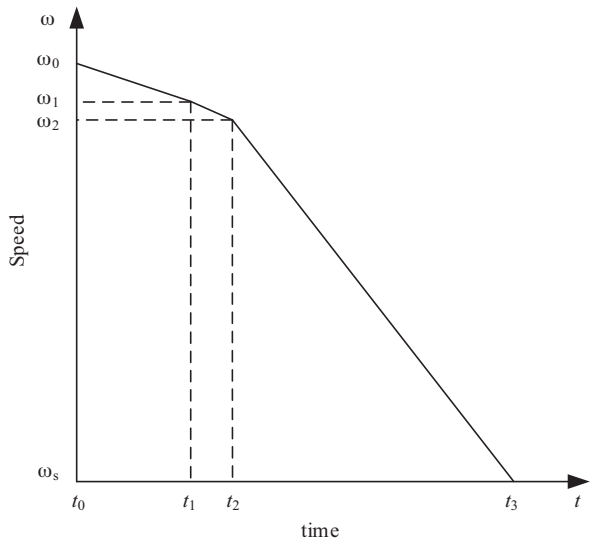

Figure 3. Detailed idling process of synchronous condenser rotating speed without control.

If the influence of the excitation current transition process is neglected, the unit loss is related to the rotational speed and can be considered as approximately constant near the rated rotational speed. The excitation loss is related to the excitation current. Under the condition of maintaining the no-load rated excitation current, the excitation loss remains basically unchanged, and consequently the total unit loss remains essentially constant around the rated speed. Therefore, it can be considered that the slope of the rotation speed remains unchanged in the progression from main excitation output no-load rated excitation current to rated rotation speed.

In the whole idling speed process, the phase angle difference between the unit and grid voltage is the integral of the frequency difference. If the unit is not connected to the grid before 3000 rpm, the phase angle difference can be considered as equivalent to the area of the graph enclosed by the curve and the horizontal axis.

Setting the grid voltage fruency to $f_0 = 50Hz$, the phase of the grid voltage vector can be determined by

$$\Phi_G(t) = \omega_s t = 2\pi f_0 t. \tag{1}$$

The phase of the voltage vector at the high voltage side of the main transformer is expressed as

$$\Phi_M(t) = \int_0^t 2\pi f_m(t)\,dt = 2\pi(f_1 - \frac{k}{2}t)t + \Phi_0, \tag{2}$$

where $f_m(t) = (f_1 - kt)$ is the unit frequency (Hz); f_1 is the frequency of the synchronous condenser when the SFC logs out; because the SFC system drags the unit to a 105% rated rotating speed, the default value of f_1 is $52.5Hz$; k is the idle speed slope of the unit; and $\Phi_0 \in [0, 2\pi)$ is the initial included angle between the main transformer high voltage side and the grid side voltage vector at the SFC exit. Thus, it can be determined that the angle difference changes with time as follows:

$$\Delta\Phi(t) = \Phi_M(t) - \Phi_G(t) = 2\pi(f_1 - \frac{k}{2}t)t + \Phi_0 - 2\pi f_0 t = 2\pi\left[(f_1 - f_0)\,t - \frac{k}{2}t^2\right] + \Phi_0, \tag{3}$$

where $k = (52.5 - 50)\,Hz/17s = 5/34Hz/s$, and $t = (f_1 - f_m)\,/k$. After substitution, we obtain

$$\Delta\Phi(f_m) = 2\pi \times 3.4 \times \left[-f_m^2 + 100f_m - 52.5 \times 47.5\right] + \Phi_0 \tag{4}$$

simplicity, both sides are divided by 2π to yield

$$\Delta\Phi(f_m) = 3.4 \times \left[-f_m^2 + 100f_m - 52.5 \times 47.5\right] + \Phi_0, \tag{5}$$

where $\Phi_0 = \Phi_0/2\pi \in [0, 1)$.

Thus, the phase difference at different moments is affected by the speed change rate and initial phase difference. Therefore, with the change in initial angle difference, the synchronous grid-connection situation will also change.

3.2. Analysis of grid-connection impact

Based on the analysis in section 2.1, since the initial state of each grid connection is different, the grid-connection state will also vary. This section simulates the influence of various angle differences and frequency differences on the grid-connected impact of a 300 MVAR synchronous condenser. When the grid-connection angle difference is fixed at 1°, changing the grid-connection frequency difference yields the results listed in Table 1.

When the grid-connection angle difference is small, the impact current amplitude is proportional to the grid-connection frequency difference because the maximum impact current occurs in the grid-connection drive process. In contrast, when the grid-connection frequency difference decreases to a certain extent, the impact current does not decrease linearly due to the angle difference. Under the condition of a fixed grid-connection angle difference of 2°, a frequency difference of $0.12Hz$ causes an impact current of 0.218 pu, and a frequency difference of $0.22Hz$ causes an impact current of 0.219 pu. That is, the impact current essentially does not change.

Under the condition of a fixed grid-connection frequency difference of $-0.475Hz$, the relationship between impact current and angle difference is obtained as shown in Table 2. In this case, the frequency difference determines the minimum impact current. As the angle difference increases, the impact current increases in an approximately linear relationship.

Based on these simulations, an increase in the grid-connection frequency and angle differences will affect the grid-connection impact current. In order to reduce the impact of the synchronous condenser grid connection on the system, the grid-connection frequency and angle differences should be reduced.

Table 1. Impact of frequency difference at a constant angle difference.

Frequency difference /Hz	0.600	0.547	0.317	0.267	0.230	0.158
Impact current /pu	0.311	0.278	0.166	0.154	0.141	0.111

Table 2. Impact of angle difference at a constant frequency difference.

Angle difference /Hz	0.1°	2°	5°
Impact current /pu	0.254	0.300	0.440

3.3. Analysis of grid-connection synchronous window

According to Equation 5, an expression for unit frequency depending on angle difference can be obtained:

$$f_m = 50 \pm \frac{\sqrt{25 - 4\left(\Delta\Phi - \Phi_0\right)/3.4}}{2}. \tag{6}$$

The angle difference at $50Hz$ can also be deduced according to Equation 5:

$$\Delta\Phi\left(50\right) = 21.25 + \Phi_0. \tag{7}$$

Thus, the zero-angle-difference grid-connection point closest to $50Hz$ is $\Delta\Phi(f_m) = 22$ when $\Phi_0 \geq 0.75$. According to Equation 6, the maximum frequency difference for this case is

$$max(f_m - 50) = max(\frac{\sqrt{25 - 4(22 - \Phi_0/3.4)}}{2}) = 0.271 \tag{8}$$

When $\Phi_0 < 0.75$, the zero-angle-difference grid-connection point closest to $50Hz$ is $\Delta\Phi(f_m =) = 21$. According to Equation 6, the maximum frequency difference for this case is

$$max(f_m - 50) = max(\frac{\sqrt{25 - 4(21 - \Phi_0/3.4)}}{2}) = 0.542 \tag{9}$$

By comparing equations 8 and 9, it can be seen that, under the condition of a fixed idling rate of 0.147 Hz/s, the maximum possible frequency difference is 0.542 Hz. Therefore, the grid-connection condition of the synchronous device should be greater than 0.542 Hz.

When the allowable grid-connection frequency difference is greater than 0.6 Hz, there must be a synchronous point, and the duration of the window at each synchronous point should be considered. This special case is indicated by the black curve in Figure 4, where there are three grid-connection nodes: P1, P2, and P3. Considering $\pi kt^2 = \Delta\theta$, the optimal grid-connection window near P3 is $T_{out} = 2\sqrt{\Delta\theta/\pi k}$. If the grid allows an angle difference of 5° and idling speed of $k = 5/34$, then the optimal window length is equal to 869 ms.

Next, consider the duration of synchronous windows T_1 and T_2, which can be calculated as follows:

$$T_1 = T_2 = \sqrt{\frac{2\pi + \Delta\theta}{\pi K_2}} - \sqrt{\frac{2\pi - \Delta\theta}{\pi K_2}} = 51ms. \tag{10}$$

Because the trajectory curve moves up and down with the changing initial phase angle difference, there may be no "optimal synchronous window," as indicated by the blue, green, and purple dotted lines where T_1 and

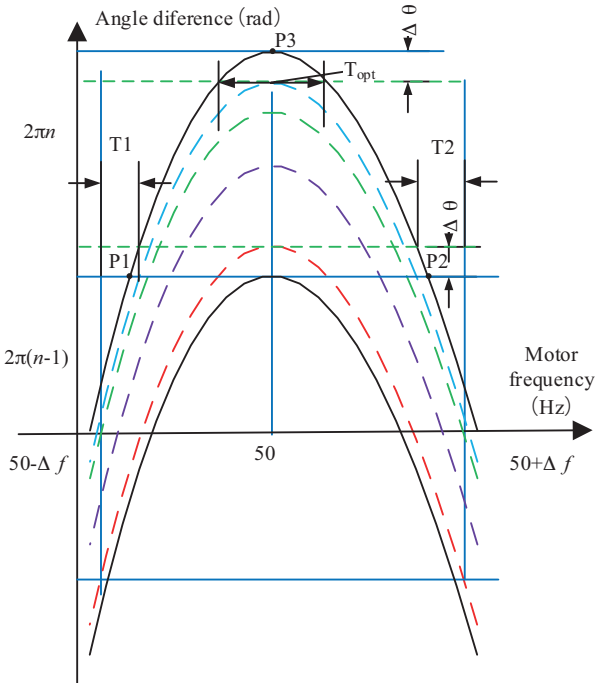

Figure 4. Schematic diagram of the synchronization window represented using the angle difference at a given condenser frequency.

T_2 are the worst cases. Therefore, the synchronous device should ensure that the duration of the synchronous window is greater than 51 ms. If the grid-connection angle difference requirement is relaxed, the duration of the synchronous window can be increased.

4. Grid-connection optimization strategy

According to the analyses thus far, in order to ensure a high grid-connection success rate, stricter requirements regarding setting the synchronous window and grid-connection frequency difference of synchronous devices are required. At the same time, when the grid-connection frequency difference is large, the impact on the power grid is relatively large. Thus, it is necessary to develop and optimize the grid-connection strategy to simultaneously improve the grid-connection success rate and reduce the grid-connection impact current.

4.1. Effect of idling rate on grid connection

The idling process of the unit can be simulated by software according to actual electrical, mechanical, and loss parameters. The idling speed times were set as 15 s, 17 s, 20 s, and 25 s (105% to 100% of the rated rotational speed time), and the initial angle difference was set as zero. The curves of the angle difference with respect to frequency at different idling rates are shown in Figure 5.

Based on Figure 5, when the idling rate is high, that is, when the idling time is long, the curve passing through the frequency segment corresponding to $2n\pi$ to $2(n+1)\pi$ is small, ensuring that the frequency difference range of the existing grid-connection node is also small. On the contrary, when the idling rate is high and the idling speed time is short, the curve passing through the frequency segment is large, ensuring that the frequency difference range of the grid-connection point is also large. A change in the initial value may result in a grid

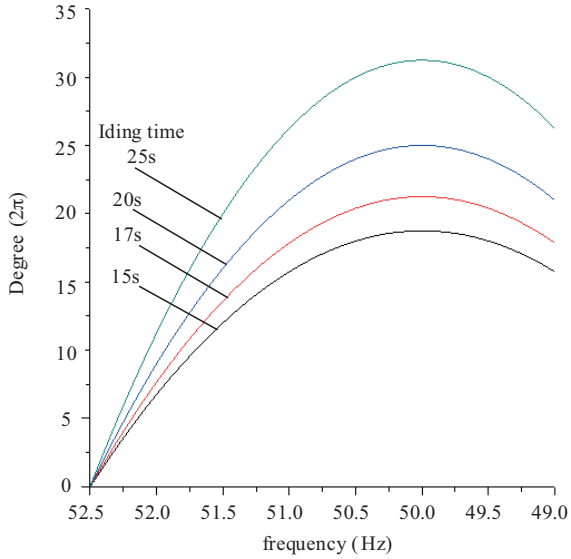

Figure 5. Curves of the angle difference with respect to frequency at different idling rates

connection with a large frequency difference. Therefore, the grid-connection conditions can be changed according to the system idling rate.

4.2. Optimization strategy for idling grid connection

The goal of optimal grid connection should be to achieve a frequency difference and angle difference both equal to zero, which is the best grid-connection point. When the excitation current is equal to 0, the system idling speed is low due to the small loss. When the excitation current completes the voltage construction, the system idles with an approximate slope of k. Therefore, the optimized grid-connection strategy can be obtained as shown in Figure 6.

In the transition process, the unit idles with an excitation current close to the no-load rated excitation current. From t_2 to t_{op0}, the sampling value of the idling rate is obtained by sampling the condenser rotation speed and performing a calculation. The angle difference between the synchronous condenser and the system at t3 can then be estimated based on this value. According to equation 3, an expression for the angle difference at t_3 can be obtained as follows:

$$\Delta\Phi(t_3) = \int_{t_2}^{t_3} \omega \, dt + \Phi_0 = \frac{1}{2}\frac{\omega_2 - {\omega_s}^s}{k} + \Phi_0(t_{opt}), \tag{11}$$

where $\Phi_0(t_2)$ is the angle difference at moment t_2, and $\Delta\Phi(t_3)$ is the expected angle difference. From the previous analysis, when the expected angle difference is 0, the system will be connected to the grid under the optimal condition. On the other hand, if the expected angle difference is large, the point at which the grid-connection angle difference is equal to zero will be farther from 50 Hz, and the grid-connection frequency difference will be large.

Therefore, if the expected angle difference is larger than a set value, the system enters the optimization program at t_{opt} and reduces the excitation current to k_1 times the rated value. As the excitation current

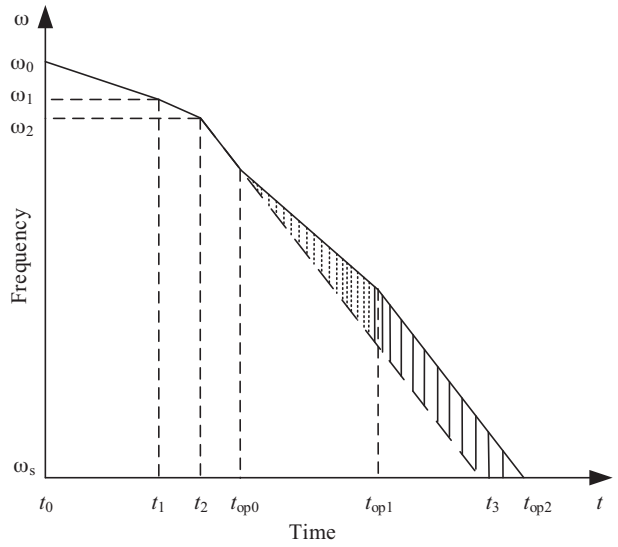

Figure 6. Multislope velocity curve with the optimized idling grid-connection strategy.

decreases, the system idling speed will also decrease. As shown by the solid line in Figure 6, the angle difference will increase as the system idling speed process increases. If the expected angle difference in Equation (11) is kept unchanged, an expected angle difference of 50 Hz can be obtained after the excitation current is restored to the rated excitation at each moment. Assuming the expected angle difference of the system at time t_{op1} is $2n\pi$, at this moment, the excitation current is restored to the rated value, and the voltage is rebuilt. According to previous analyses, the change in angle difference caused by rotation speed is equivalent to the area of the graph, and thus the increase in angle difference can be regarded as equivalent to the area of the shaded part of the graph in Figure 6.

4.3. Optimization algorithm implementation

According to Equation 11, an expression for judging whether there is a synchronous point can be obtained as follows:

$$\begin{cases} \left|\Phi_0(t_{opt}) + \int_{t_{opt}}^{T} (\Delta f_{t_{opt}} + k_0 t)\, dt\right| < \Delta\theta_{set} \\ \left|\Delta f_{t_{opt}} + k_0 T\right| < \Delta f_{set} \end{cases} \tag{12}$$

If a T can be found to satisfy Inequality 12, no adjustment is required for this grid connection. If no feasible solution can be found, there is no grid-connection point that simultaneously meets the frequency difference and angle difference requirements for grid connection. If there is no such connection point, the excitation current is adjusted to 0.5 times the no-load rated current at time t_{op0}. Because of the decrease in excitation current, the unit loss and idling speed decrease.

As it is difficult to solve simultaneous inequalities, equation 12 is converted into

$$\begin{cases} \left|\Phi_0(t_{opt}) + \int_{t_{opt}}^{T} (\Delta f_{t_{opt}} + k_0 t)\, dt\right| = \Delta\theta_{set} \\ \left|\Delta f_{t_{opt}} + k_0 T\right| < \Delta f_{set} \end{cases} \tag{13}$$

If there is no solution to Inequality 13, the excitation current is adjusted. After the excitation current is adjusted to 0.5 times the no-load rated current, the goal of the adjustment becomes to find a time top1 at

which the excitation current is adjusted back to the no-load rated current. Then, there can be a synchronous point that meets the frequency difference and angle difference requirements. That is, the problem that satisfies Inequality 14 must be solved.

$$\begin{cases} \left|\Delta\theta_{op0} + \int_{t_{op0}}^{t_{op1}} (\Delta f_{op0} + k_0 \frac{0.25Q_{cu2}+Q_m}{Q_{cu2}+Q_m} t)\, dt + \int_{t_{op1}}^{T_1} k_0 t\, dt\right| < \Delta\theta_{set} \\ \left|\Delta f_{t_{opt}} + k_0 T\right| < \Delta f_{set} \end{cases} \tag{14}$$

Again, it is difficult to solve simultaneous inequalities, and electrical and mechanical losses cannot be obtained in advance. Therefore, in order to facilitate the program implementation, Inequality 14, which is solved to obtain t_{op1}, is converted to Inequality 15, which is solved in real time. When T_1 satisfies Inequality 15, after the excitation current is restored to the no-load rated current at that moment, a synchronous point can be found to meet the grid-connected frequency difference and angle difference requirements.

$$\begin{cases} \left|\Delta\theta_{op0} + \int_{t_{op1}}^{T_1} (\Delta f_{op1} + k_0 t)\, dt\right| = \Delta\theta_{set} \\ |\Delta f_{op1} + k_0 (T_1 - t_{op1})| < \Delta f_{set} \end{cases} \tag{15}$$

Assuming that the current time is t_{op1}, if the excitation current is adjusted to the no-load rated current, there should be a synchronous point that satisfies Inequality 13 under the condition of the idling speed being in the no-load rated excitation current state. That is, it can be confirmed whether the current time is top1 by solving Inequality 15. If the current time is t_{op1}, the excitation current will be adjusted back to the no-load rated value, and the optimization will end. If the current moment does not meet Inequality 15, then the excitation current is maintained at 0.5 times the no-load rated value, and Inequality 15 is judged again at the next moment.

The flowchart of the optimization algorithm is shown in Figure 7.

5. Simulation and RTDS simulation results

To verify the effectiveness and feasibility of the proposed method, simulations are build. And the main parameters of the new generation SC are listed in Table 3.

Table 3. Main parameters of SC.

Parameter	Value
Rated capacity	300 Mvar
Rated loss	3245 kW
Rated voltage	20 kV
Rated current	8660 A
Rated frequency	50 Hz
Rated speed	3000 r/min

5.1. Simulation comparison

Through MATLAB simulation software, start-up and grid-connection simulations of the synchronous condenser were conducted, and the optimization algorithm and the traditional algorithm were respectively simulated.

In order to reduce the simulation time, the idling speed of the two units was initially set to 3090 rpm, and the excitation subsequently built up. The initial angle difference between the two units and the grid voltage

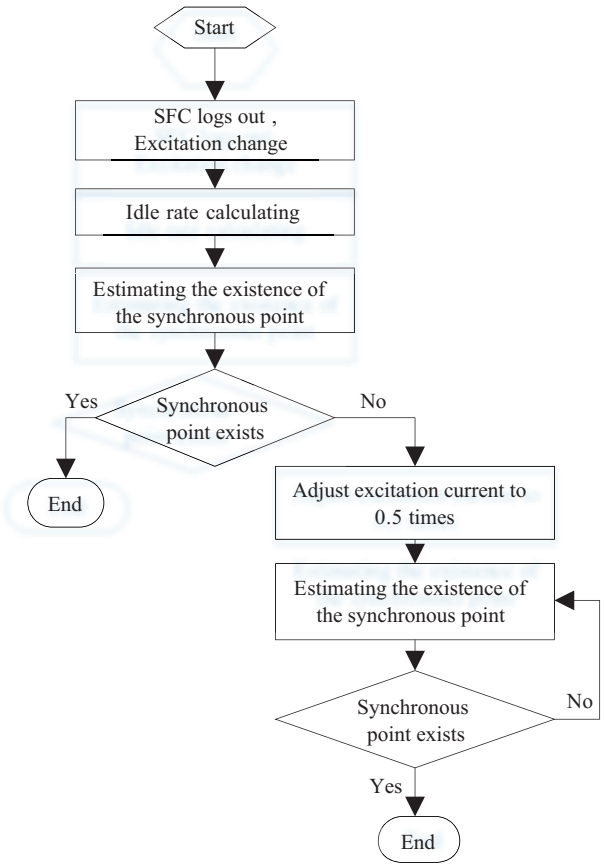

Figure 7. Flowchart of the optimized idling grid-connection strategy.

was $100°$, the allowable angle difference of grid connection was $2°$, and the allowable frequency difference of grid connection was $\pm 0.4Hz$. The simulation results are shown in Figure 8.

It can be determined from the simulation results that, when the optimal idling speed is not adopted for grid-connection, the grid-connection speed of the unit under this condition is 3022.1 rpm, and the grid-connection frequency difference is 0.368 Hz. After the optimal idling speed is adopted, the grid-connection time increases, and in the period of downward adjustment of excitation, the idling rate decreases significantly, and the final grid-connection speed is 3010.4 rpm, and the grid-connection frequency difference is 0.173 Hz.

Meanwhile, the amplitude of the three-phase impulse current vectors flowing through the grid-connected switch at the high voltage side of the main transformer is as shown in Figure 8b.

The impact of grid-connection is not only determined by frequency difference, but also affected by angle difference. However, through the optimization algorithm, when the fixed grid-connection angle difference is $2°$, the impact current amplitude of the optimization algorithm is 144.8 A, which is 16.6% lower than the 168.9 A without the optimization algorithm.

The goal of the optimization algorithm is to make the unit connected to the grid have zero frequency difference. Compared with the theoretical calculation, the actual excitation regulation needs time; the excitation regulation process will affect the result of the optimal idling speed, and the final frequency difference will fall between $\pm 0.2Hz$. Compared with the traditional algorithm, the optimal idling speed grid-connection algorithm

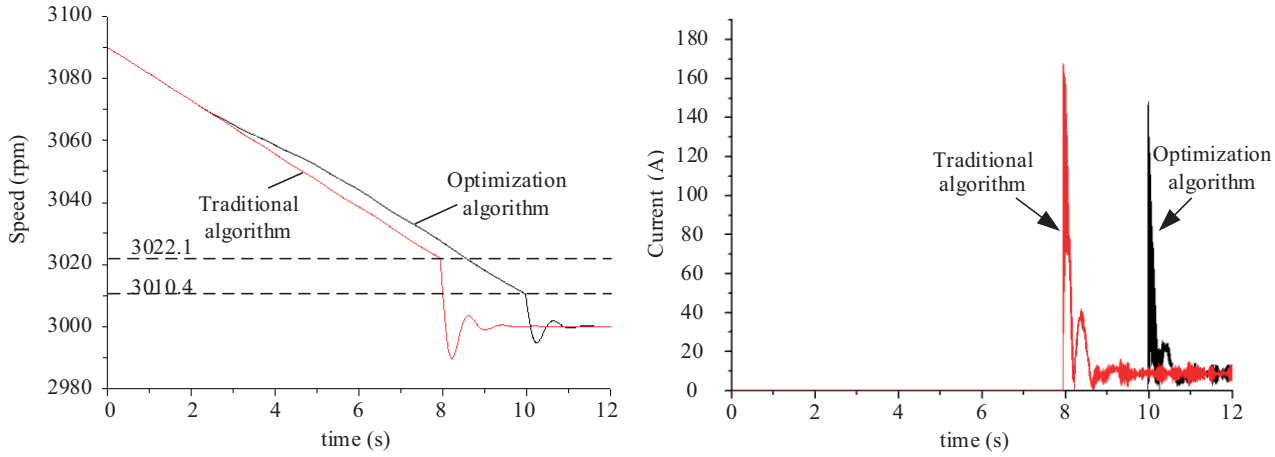

Figure 8. Comparison result of idling grid-connection between the traditional and the optimization algorithms.

can reduce the allowable frequency difference by more than 50%, effectively reducing the power impact resulting from idling speed grid-connection.

5.2. RTDS simulation results

A synchronous condenser RTDS test platform was constructed based on an existing platform, and the optimized grid-connection strategy was verified. As shown in Figure 9, the platform includes RTDS real-time digital emulator, IO interface card and controller. The IO card completes the mutual conversion of digital and analog signals; the RTDS real-time digital emulator and IO card are connected through optical fiber, and the signal interface card is connected with the control and protection equipment cable. The power supply, primary circuit, motor and excitation system of the static inverter are realized in the form of digital model in the simulator of RTDS; the digital signals of the voltage, current and breaker state of the primary part of the simulation are output to the controller through the interface board; according to these values, the controller takes the speed as the control object, and outputs the trigger pulse of SFC.

The obtained test results are shown in Figure 10. Based on the experimental results, when the voltage construction is completed, the system will reduce the excitation current, and the idling speed will change after a sampling time of 2 s.

When the expected angle difference meets the requirement, the system rebuilds the voltage and finally connects to the grid at 3000 rpm. The frequency difference is approximately zero and the measured value is $0.09Hz$. After applying the grid-connection optimization strategy, the grid frequency difference could be optimized from $0.54Hz$ to $0.3Hz$ and the grid-connection angle difference from 5° to 2°. With decreasing grid frequency and angle differences, the synchronous condenser idling grid-connection impact decreases significantly.

From the results of the RTDS simulation test, when the excitation current is fixed, the idling rate is approximately unchanged, and with a change in excitation current, the idling rate also changes accordingly; thus, we can correct the grid-connected frequency difference. When the grid-connection frequency difference is small, the synchronous window increases, which aids the synchronous device in reducing the grid-connection angle difference and impact current.

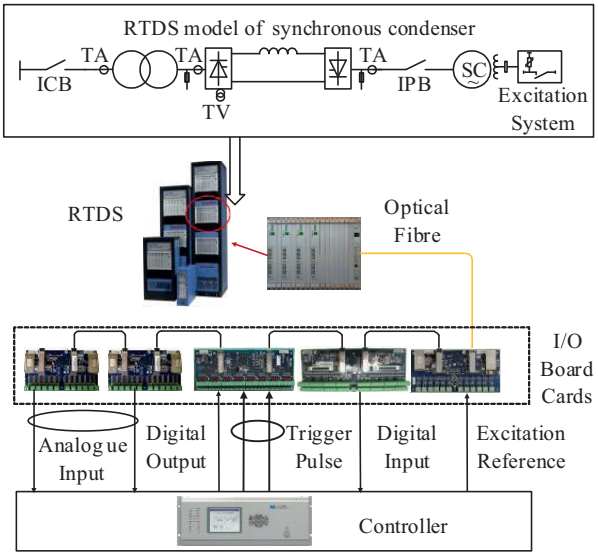

Figure 9. RTDS platform configuration of the synchronous condenser system.

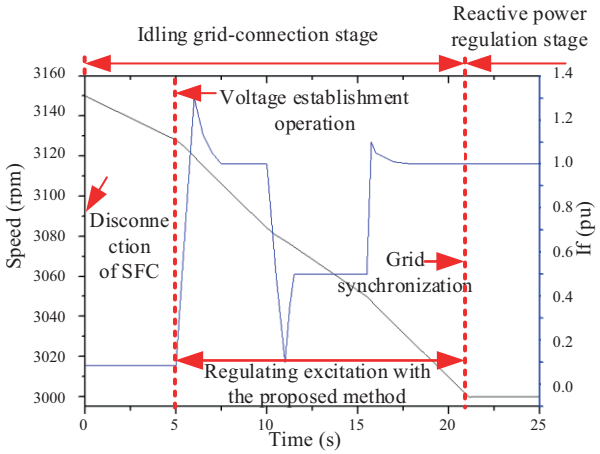

Figure 10. RTDS test results of the proposed optimized idling grid-connection strategy.

6. Conclusion

The new generation of synchronous condensers can effectively alleviate the dynamic reactive power shortage problem caused by strong HVDC systems, weak AC systems, and large load centers. During the grid-connection process of the new generation of synchronous condensers, there is a stage without prime power dragging, during which a series of processes such as excitation switching and synchronous grid-connection must be completed. This introduces new requirements for synchronous condenser grid connection.

This paper analyzed the grid-connection process of the synchronous condenser idling speed and provided a basis for setting the parameters of the synchronous device. Furthermore, an optimized idle speed grid connection strategy was proposed, and its effectiveness proved by RTDS testing. The strategy can significantly reduce the grid-connection frequency and angle differences and decrease the impact of the 300 MVAR synchronous grid connection on the system.

Acknowledgment

The work is supported by the National Natural Science Foundation of China (No. 51877042).

References

[1] Fan X, Zhou Y, Ruan L, Zhou K, Wang T et al. Study on coordinated control strategy of reactive power compensation device in DC converter station with new-generation synchronous condensers. In: 2018 International Conference on Power System Technology; Guangzhou, China; 2018. pp. 2966-2971.

[2] Ramachandra SK, Vinoth KN, Harada Y. Impact of renewable energy control center on voltage stability and transmission network efficiency in wind farm integrated grid. In: 2014 IEEE International Conference on Power Electronics, Drives and Energy Systems; Mumbai, India; 2014. pp. 1-6.

[3] Wang X, Wei X, Meng Y. Experiment on grid-connection process of wind turbines in fractional frequency wind power system. IEEE Transactions on Energy Conversion 2015; 30 (1): 22-31. doi: 10.1109/TEC.2014.2358498

[4] Givaki K, Rahman HM, Vozikis D, Giveki. A. Analysis of integration of multi-terminal HVDC network to weak grids. The Journal of Engineering 2019; 2019 (16): 3219-3224. doi: 10.1049/joe.2018.8447

[5] Rabiee A, Soroudi A, Keane A. Risk-Averse preventive voltage control of AC/DC power systems including wind power generation. IEEE Transactions on Sustainable Energy 2015; 6 (4): 1494-1505. doi: 10.1109/TSTE.2015.2451511

[6] Pu Y, Zhong Q, Li X, Hu Y, Xu G. In: Influence of synchronous condenser on voltage stability of HVDC. In: 2018 IEEE Power & Energy Society General Meeting; Portland, OR, USA; 2018. pp. 1-5.

[7] Zhuang Y, Menzies RW, Nayak OB, Turanli. HM. Dynamic performance of a STATCON at an HVDC inverter feeding a very weak AC system. IEEE Transactions on Power Delivery 1996; 11 (2): 958-964. doi: 10.1109/61.489357

[8] Kalsi SS, Madura D, Ingram M. Superconductor synchronous condenser for reactive power support in an electric grid. IEEE Transactions on Applied Superconductivity 2005; 15 (2): 2146-2149. doi: 10.1109/TASC.2005.849481

[9] Fan X, Zhou Y, Ruan L, Zhou K, Wang T et al. Study on transient reactive power characteristics of new-generation large synchronous condenser. In: 2018 China International Conference on Electricity Distribution; Tianjin, China; 2018. pp. 1851-1855.

[10] Wu M, Dong Z, Li P, Ma X, Jin Z et al. Impact of new-type synchronous condenser on voltage stability of jarud sending-end system. In: 2018 International Conference on Power System Technology; Guangzhou, China; 2018. pp. 2654-2659.

[11] Rather ZH, Chen Z, Thøgersen P, Lund P. Dynamic reactive power compensation of large-scale wind integrated power system. IEEE Transactions on Power Systems 2015; 30 (5): 2516-2526. doi: 10.1109/TPWRS.2014.2365632

[12] Teleke S, Abdulahovic T, Thiringer T, Svensson J. Dynamic performance comparison of synchronous condenser and SVC. IEEE Transactions on Power Delivery 2008; 23 (3): 1606-1612. doi: 10.1109/TPWRD.2007.916109

[13] Wang Q, Li T, Tang X, Liu F, Lei J. Study on the site selection for synchronous condenser responding to commutation failures of multi-infeed HVDC system. The Journal of Engineering; 2019 (16): 1413-1418. doi: 10.1049/joe.2018.8807

[14] Ryu H, Kim B, Lee J, Lim I. A study of synchronous motor drive using static frequency converter. In: 2006 12th International Power Electronics and Motion Control Conference; Portoroz, Slovenia; 2006. pp. 1496-1499.

[15] Chai X, Zhang C, Wang Y, Gao J, Yang H. Analysis on idle-load grid-connection transient impact current of DFIG. In: 2011 International Conference on Electrical Machines and Systems; Beijing, China; 2011. pp. 1-5.

[16] Wang P, Mou Q, Liu X, Gu W, Chen X. Start-up control of a synchronous condenser integrated HVDC system with power electronics based static frequency converter. Access 2019; 7 (1): 146914-146921. doi: 10.1109/IFEEC.2017.7992178

[17] Wang P, Liu X, Mou Q, Gu W, Zhao X. Start-up control and grid integration characteristics of 300 MVar synchronous condenser with voltage sourced converter-based SFC. Access 2019; 7 (1): 176921-176934. doi: 10.1109/ACCESS.2019.2953052

[18] Yang H, Zheng Y, Wang X, Jian Y, Hu J. Calculation method of success rate for idling grid-connection of large synchronous condensers. Automation of Electric Power Systems 2018; 42 (24): 74-78. doi: 10.7500/AEPS20180320003

[19] Zhang H, Hasler J, Johansson N, Ängquist L, Nee H. Frequency response improvement with synchronous condenser and power electronics converters. In: 2017 IEEE 3rd International Future Energy Electronics Conference and ECCE Asia; Kaohsiung, Taiwan; 2017. pp. 1002-1007.